WELD TRACK DISTORTION IN LASER POWDER BED FUSION OF NICKEL SUPERALLOY 625

Jason C. Fox[1], Chris J. Evans[1,2], Aarush Sood[2] Romaine Isaacs[3*], Brigid Mullany[2], Angela Davies Allen[2], Ed Morse[2]

[1]National Institute of Standards and Technology, Gaithersburg, MD 20899, USA[†]
[2]University of North Carolina at Charlotte, Charlotte, NC28223, USA
[3]Carl Zeiss Industrial Metrology LLC, Knoxville, TN 37932

Laser powder bed fusion (LPBF) is one of a group of manufacturing technologies capable of producing complex structures and surfaces in small batches and with reduced lead time. Materials ranging from light metals (e.g., aluminum alloys) to high temperature alloys can be used. This work focuses on nickel super alloy 625 (IN625) and explicitly on characterization of surfaces that are subsequently covered by additional layers. The surface features described here – double wide solidified "weld tracks" that occur both on sides of stripes and at part edges, and large scale deformations of solidified melt pools at intersections of part features – have not, to our knowledge, been previously described in the literature. The lateral and vertical scales are such that powder layer thickness will be significantly modulated while spreading the next layer of powder. This is likely to affect local material properties in the subsequent layer(s).

Experimental Methods

Two sample sets were built on an EOS M290 using parameters recommended by the machine and powder vendor, with the following exception: the "upskin" feature, which adapts process parameters in the final layers to improve surface finish, was turned off in both builds. Hence the top surfaces are representative of upward facing features in the body of the build.

The first set built in 2017 and described elsewhere [1] has ten samples 38 mm x 40 mm x ≈ 5 mm, built on a subplate. The samples were built like a staircase, with an 8 mm wide reference area followed by eight single-layer (40 μm high) steps. Variables were orientation, location in the build, and stripe width, which was set to default in the second set.

The second set compises 12 samples, each measuring 25 mm x 20 mm x ≈ 10.6 mm and built on a subplate in 2019. Leaving aside a region at each end of the sample, additional layers were added to build five, 40 μm tall steps of 20 mm x 4 mm on each of the 12 samples. Most of the 12 samples added one layer (i.e., 40 μm) per step, with variations of location and orientation with respect to argon flow within the build. A few used more layers per step (e.g., multiples of 40 μm). Analysis here does not include the effect of step size as all twelve samples showed distortions of the solidified weld tracks discussed here. Additionally, all the observations reported here have been made using samples from the second set. The earlier set of samples [1] have recently been remeasured and show similar features to those reported here.

TABLE 1: Nominal build conditions:

Laser power	285 W
Velocity	960 mm/s
Powder	EOS IN625; D50 = 27.1 μm
Layer thickness	40 μm nominal
Step over	110 μm
Stripe width	10 mm

Surface characterizations reported here are based on scanning electron microscope (SEM) and/or Zygo ZeGage Plus or NexView coherence scanning interferometers (CSI) with, in both cases, 20x and 50x Mirau objectives. Data processing on the CSI instruments uses native software (Mx version 8.0.0.26). SEM images

[*] *Now at Intel, Beaverton, OR*

[†] Certain commercial entities, equipment, or materials may be identified in this document to describe an experimental procedure or concept adequately. Such identification is not intended to imply recommendation or endorsement by the National Institute of Standards and Technology, nor is it intended to imply that the entities, materials, or equipment are necessarily the best available for the purpose.

were acquired on a ZEISS GEMINI SEM 450 using an in-lens Secondary Electron (SE) detector. Further details are given in [2] and [3].

A subset of the features we observe have been reported elsewhere [4-5]. In [2] we described previously unreported surface features in layers that ultimately become part of the "bulk" with lateral dimensions ranging from tens of nanometers to hundreds of micrometers. In some cases, these features may affect the build of the subsequent layer, although remelting may diminish that effect.

Here we focus on meso-scale distortions of the solidified weld track. These distortions arise from a combination of part design and the default scanning strategy for IN625 in the EOS M290. Some of these distortions have amplitudes greater than the nominal thickness of the next layer or cause localized denudation, increasing the thickness of the next powder layer.

The features discussed here were located in part coordinates using stitched SEM images, part build data, or optical inspection. The in-built scan lines for establishing the sample coordinate system allows high resolution registration of features between metrology systems [2].

The global coordinate system was written in situ on the sub plate as a set of single track scan lines. For every "step" on every sample, a coordinate reference was built at the edge of the layer (Fig 1) in fused material. The laser power turns off at the edge of the coordinate system for that layer, leaving a region that is still molten for a brief moment. When this solidifies, it leaves an imprint reflecting the melt pool dimensions.

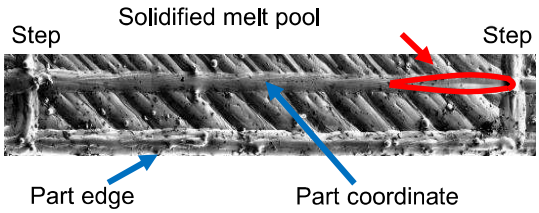

Fig 1. Stationary melt pool solidifies leaving an indication of melt pool dimensions.See also Fig 6 Stitched SEM. Horizontal distance between steps is 4 mm.

Preliminary measurements of six such stationary solidified melts pools were made manually on three samples (with a resolution of 0.1 mm) using the ZeGage Pro data. Mean melt pool length, measured from tip to tail, is (1.15 +/- 0.15) mm (mean +/- half the range), which includes both fabrication process variations and Type A measurement uncertainties.

STRIPES AND EDGES

Measurements of LPBF surfaces commonly show an elevated "weld track" bounded by furrows at a regular spacing given by the laser step over (H in Fig. 2). Lower amplitude linear structures may be observed, reflecting the wake of the solidifying melt pool [1,5]. Larger scale signatures occur at turnarounds where we observe a doubling of the track width.

Default build parameters in the EOS M290 for IN625 include a stripe width (S, maximum travel of the laser spot before reversing direction). At these locations there is potential for a "hot turnaround" (i.e., where the end of the previous track is still molten or hot enough to be remelted), which result in double wide solidified weld tracks (see Fig. 2). Consider the laser turning on at time t=0 to start fusing metal powder (Fig 2(i)) at x(0)y(0) and traveling at fixed speed and power to x(0)y(S) where the laser is turned off, leaving hot metal for some distance in the -y direction. At time t_n the laser has turned back on at x(H)y(S) (Fig 2(iii)) fusing metal powder again in the -y direction (Fig 2(iii)). Over some distance (toward Fig 2(iv)) the available energy is sufficient to produce a double wide melt pool. Suface tension increases as the metal cools, giving increased peak height, limited by available molten metal. The resulting length of "Double-wide" varies. Another "Double-wide" section is generated in some area area approaching x(2H)y(0) (i.e., Fig 2.v) This cycle repeats producing "double-wide' melt pools at all turn arounds for x=0 to x_{max} (the layer width) originating at y(0) and y(S).

A stripe boundary is constructed from the confluence of two turnaounds. "Stripe overlap" controls how far beyond Y=S toward Y=2S (for example) the laser travels, resulting in a futher "build up" at the stripe. A CSI height or intensity map, or an SEM image reveals which layer was fused first (Figs 3 and 4).

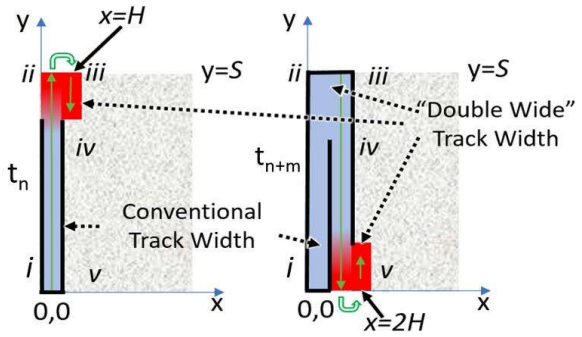

Fig 2. Conceptual map of the formation of double-wide solidified weld tracks orthogonal to laser scan direction

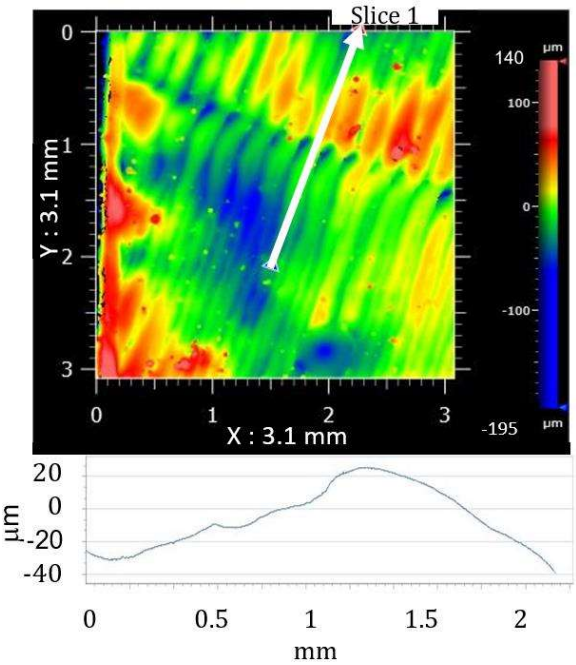

Fig 3. Top: Height map through stripe showing double *wide solidified weld tracks at stripe boundaries (upper 1/3rd) and at edge of part on left side. Bottom: Slice 1 profile showing height variation across stripe. (Zygo ZeGage Pro, 20x Mirau obj.,9x9 stitch, 20% overlap)*

Fig 3 also shows variation in double wide tracklengths on both sides of a stripe. Over the population of the second generation sample that have been measured, the range of double wide solidified melt pools ranges from 0.5 mm to 2 mm. This variation is likely due to local variations in heat conduction through the part into the build plate. This conduction will also vary locally based of location of part edges and other features. Other influences may include infrared (IR) coupling to the machine environment, convection via the argon flow, and vapor plume variation [7,8]. The extracted profile ("Slice 1" in Fig 3) shows height variation with respect to a best fit plane. Further work is required to assess the influence, in general, of scan strategy and part geometry on the formation of "double wide" tracks. That said, the amplitude (i.e., height) range is greater than the thickness of the next powder layer.

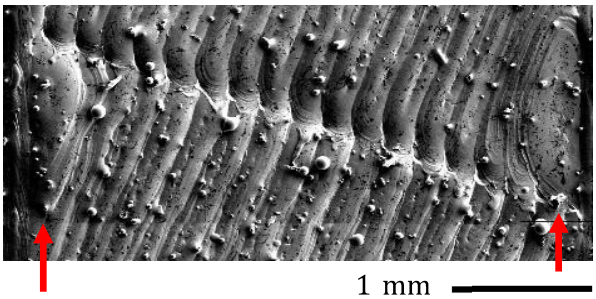

Fig 4. Stitched SEM image of a stripe boundary. Also shown (indicated by red arrows), are areas where stripes intersects the assymetic edges of steps at an included angle of ≈ 70° producing large melt pool deformations discussed below.

Fig 5 shows the effect of a stripe on subsequent fused layers. The effect of the stripe after one layer has been fused is clearly visible in the SEM data. This observation is supported by stitched CSI data along the line formed by the stripe boundary. The effect on layer 2 is hard to extract from current CSI height data; the SEM data is slope sensitive, suggesting future work looking at CSI slope data. As noted previously, there is variation in the length of the double-wide sections along stripes. In general, stripe boundaries are formed by the combination two adjacent turnarounds. Height profiles across these boundaries suggest that the peak of the double wide sections can be a significant fraction of the nominal thickness for the next layer of powder, suggesting a localized effect in fusing the next layer(s).The stripe affects at least two layers of this build.

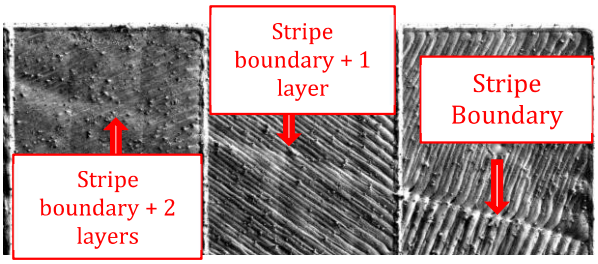

Fig 5. Stitched SEM image showing effect of a stripe boundary on subsequent layers

SOLIDIFIED MELT POOL DEFORMATIONS

In the previous section, we have discussed solidified melt pool distortions that are mostly far (comparitavely) from edges of other sources of thermal distortion. Under the default EOS M290 parameter for IN 625 builds, the laser spot direction rotates by 67° per layer. Hence, for some layers, there is a low angle convergence between between laser paths, stripes and part edges. Multiple, rapid sequential hot turnarounds result in meso-scale, distorted, solidified melt pools. Fig 6 shows SEM, height, and processed CSI intensity data for an area where a stripe and the edge of the part diverge slowly (left to right) over 4 mm. Both the SEM and CSI intensity data show a curved surface signature between the stripe and the bottom of the part with a spatial period matching the laser step over.

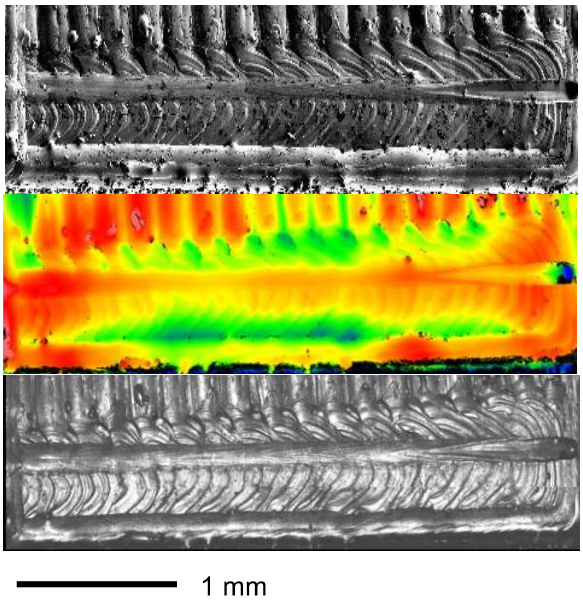

Fig 6. Top: Stitched SEM. Middle: Stitched CSI height data using ZeGage Plus 20x objective (Color range is ≈ 100 µm, where blue=low and red=high). Bottom: CSI intensity data.

Fig 7 shows a stripe diverging from a point close to the bottom edge of a part at an included angle of ≈ 35°. The intensity image (Fig 7(b)) shows distorted fine ripple in the region between the stripe and bottom edge (bounded by the red triangle). This distortion is approximately parabolic. The profile (Fig 7(c)) for slice 2 shows a periodicity close to the laser stepover (≈ 110 µm) between x = 1.5 mm and 2 mm at a lower amplitude than in a stable build. Slice 1 shows double wide tracks with a periodicity close to twice the laser stepover distance. Fig 7(a) is the denudation in the top right corner below the stripe. Fig 7(a) and (b) also show systematic variation in the distance that double-wide melt pools extend away from the stripe boundary.

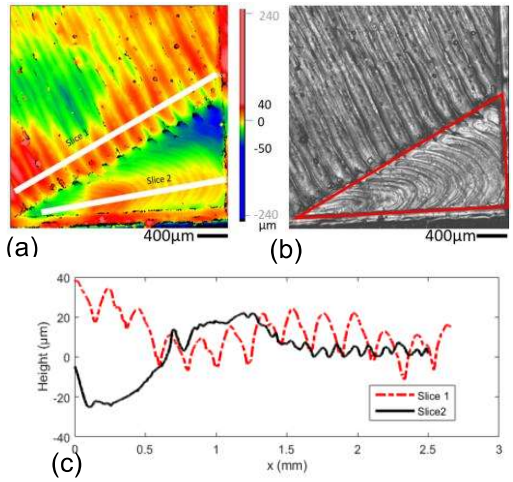

Fig 7. (a) Height and (b) intensity data showing solidified melt pool distortions where a stripe converges with a part edge. (c) Profiles for slices 1 and 2 in (a) ZeGage Plus, 20x Mirau objective, 8x8 stitch)

Fig 8 shows a different region with a large melt pool distortion. Here, a stripe on the higher step (right of upper image) intersects the step at ≈ 75°. The peak of the distorted solidified melt pool is 105 µm above the mean plane of the lower step. Put differently, the peak will protrude approximately 25 µm above the nominal level of the next layer of powder for further build on the right of the step.

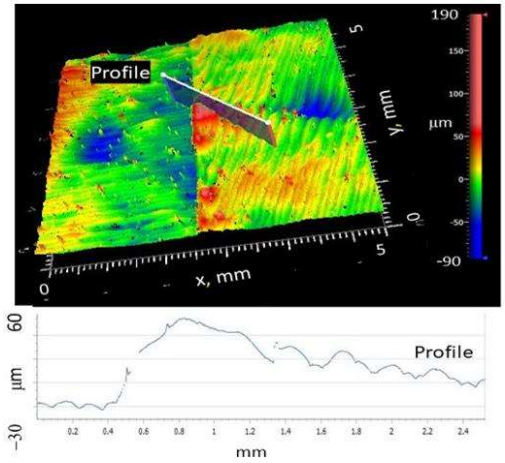

Fig.8 Solidified distorted melt pool

Figure 9 shows a stripe boundary intersecting the bottom of the sample at an included angle of ≈ 30°. The intensity image in the converging (or diverging) region (top) is similar to that in Fig 7, but the height data (middle and bottom) tells a different story. Here, the series of peaks is reminiscent of the single peak data in Fig 8. The three peaks captured here show a relatively small, but neverlethess monotonic, variation in the peak height. The peak height is extracted as a linear profile, which does not accurrately capture the independent peaks. As the separation between the stripes and the part edge increases, however, it is clear that the size of the solidfied and distorted melt pool increases.

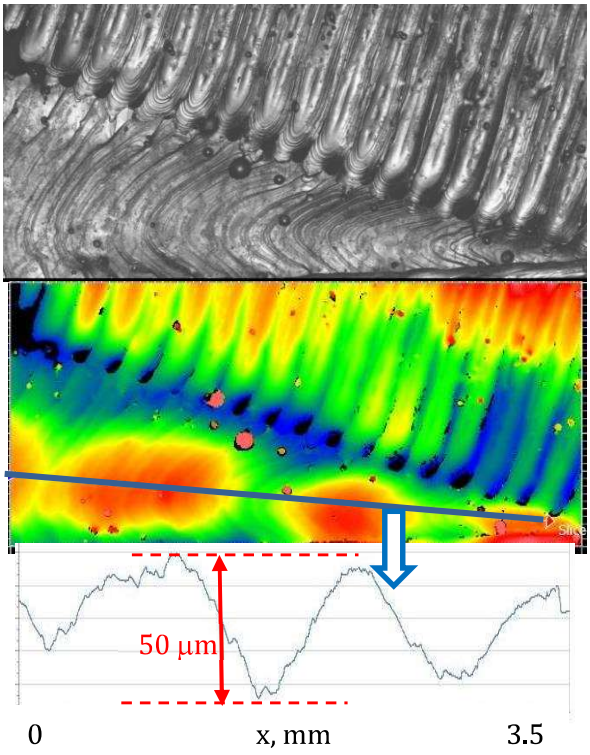

Fig 9. Periodic melt pool distortions reminescent of plateau-Rayleigh instability previously reported [9] and refered to elsewhere as "balling" [10]

CONCLUSIONS AND FUTURE WORK

In this paper, we have added to previous work [2,3] focussed on evaluating LPBF surfaces that will have additional materiel fused onto them (i.e., surfaces that will become part of the bulk). The samples used were built on a commercialy available machine using the manufacturer's recommended feedstock and parameters so that the observations are both related to on-going research and relevant to users.

In the course of the build, a coordinate system was built into every visible layer of every part and leaves a repliction of the solidifed melt pool, where we presented the range of a small sample of measured weld pool lengths. The quoted range of measurements may be taken as a conservative estimate of the Type A uncertainty, which can probably be reduced, not least by making more measurements, which will include variations in the process as well as measurement variations. The data was taken at 0.42 µm/pixel (detector limited), which could be improved by using the 50X (optics limited) objective in ZeGage, moving to the NexView system, or by using artificial iintelligence/machine learning and interpolation to identify features and evaluate length (and width). The Type B contributors that need to be evaluated include imaging distortion (likely less than 1% cubic distortion over the field of view), operator bias, and distortion due to surface tensions as the melt pool solidifies.

We have described two related types of meso-scale features that arise from "hot turnarounds": (a) double wide solidified "weld tracks" that occur on both sides of stripes and at part edges, and (b) large scale deformations of solidified melt pools at intersections of part features, stripes, and weld tracks.

A conceptual model of the formation of double-wide weld tracks [3] also provides for cooling to the point that the build reverts to two tracks. The distance at which that transition occurs varies, presumably as local cooling rates vary. We observe double wide lengths 0.5 mm – 2mm. A more rigorous definition of this transition should be developed.

We have shown that the stripes affect, at least, the next two layers of the build. The large scale deformations result from a similar mechanism in the positions on the part where turnarounds occur rapidly and multiple "tracks" merge. As these merged melt pools cool, surface tension generates high areas and denuded areas.

Our observations suggest that resulting features vary with the distances between turn arounds and the included angle between features. As an extension of this work, we have designed and built a new set of samples to evaluate these effects. They comprise a 10 mm tall pedestal built using the same parameters as the samples discussed here. The top layer is a distorted diamond and the laser track is orthogonal to the

long axis. Angles from 5° to 35° are included, as well as oblique angles at the sample waist. Fig 10 shows the built samples, as well as a close up of one pedestal and distorted diamond. All samples contain visible melt pool distortions and initial measurement results will be given in the oral presentation.

Fig 10. Top: View of a portion of the build performed. The sub-plates shown are 101.6 mm square. Bottom: Closer view of one of the sample designs. Dimensions of the sample pictured is 10 mm x 45.3 mm.

Another build is planned using pairs of samples to compare builds with fused tracks moving toward and away from specific acute angles. Additional research will also investigate the microstructure and defects (if any) in the regions of distorted weld tracks, as these areas are hypothesized to contain unwanted microstrucures and/or defects that would affect part performance.

REFERENCES

[1] Reese Z.C., Fox J.C., J. Taylor, C. Evans, Evolution of Cooling Length in Parts Created Through Laser Powder Bed Fusion Additive Manufacturing, in: Proc. 2018 ASPE Euspen Summer Top. Meet. - Adv. Precis. Addit. Manuf., Berkeley, CA, 2018: pp. 183–188

[2] Fox J.C, Allen A., Mullany B.,Morse E., Isaacs R., Lata M., Sood A., Evans C., Surface superalloy 625 additive manufacturing, in: Proc. Jt. Spec. Interest Group Meet. Euspen ASPE, St. Gallen, Switzerland, 2021

[3] Fox J.C., Sood A.,Isaacs R., Brackman P., Mullany B.A., Morse E., Allen A.D., Santos E.C, Evans C. Surface Feature Characteristics of Laser Powder Bed Fusion of Nickel Super Alloy 625 Bulk Regions> In Proc. 6th CIRP Conference on Surface Integrity, Procedia CIRP in press

[4] Senin, A. Thompson, R. Leach, Feature-based characterisation of signature topography in laser powder bed fusion of metals, Meas. Sci. Technol. 29 (2018) 045009.

[5] R.E. Ricker, J.C. Heigel, B.M. Lane, I. Zhirnov, L.E. Levine, Topographic Measurement of Individual Laser Tracks in Alloy 625 Bare Plates, Integrating Mater. Manuf. Innov. 8 (2019

[6] Z.C. Reese, J.C. Fox, F.H. Kim, J. Taylor, C. Evans, Effect of Subsurface Defects on the Surface Topography of Additive Manufactured Components, in: Proc. 2018 ASPE Euspen Summer Top. Meet. - Adv. Precis. Addit. Manuf., Berkeley, CA, 2018: pp. 127–131

[7] M. A. Stokes, S A. Khairallah, A. N. Volkov, A. M. Rubenchik. Fundamental physics effects of background gas species and pressure on vapor plume structure and spatter entrainment in laser melting. Additive Manufacturing Volume 55, July 2022, 102819

[8] S. A. Khairallah and A. Anderson. Mesoscopic simulation model of selective laser melting of stainless steel powder Journal of Materials Processing Technology, November 2014

[9] J.C. Fox, Transient Melt Pool Response in Additive Manufacturing of Ti-6Al-4V, PhD Thesis, Carnegie Mellon University, 2015

[10] J.P. Oliveir, A.D. LaLonde, J.Ma. Processing parameters in laser powder bed fusion metal additive manufacturing. Materials and Design 193, 2020

Acknowledgements

This work was funded in part by the University of North Carolina at Charlotte's Center for Precision Metrology, Zeiss, and the National Institute of Standards and Technology. J. Tarr (NIST) supported sample fabrication. G. Caskey (UNC Charlotte) supported CSI measurements. M. Fay (Zygo) provided insight into CSI metrology.